Active Disruption of an RNA-Protein Interaction by a DExH/D RNA Helicase

Eckhard Jankowsky,[1] Christian H. Gross,[2] Stewart Shuman,[2] Anna Marie Pyle[1,3]*

All aspects of cellular RNA metabolism and the replication of many viruses require DExH/D proteins that manipulate RNA in a manner that requires nucleoside triphosphates. Although DExH/D proteins have been shown to unwind purified RNA duplexes, most RNA molecules in the cellular environment are complexed with proteins. It has therefore been speculated that DExH/D proteins may also affect RNA-protein interactions. We demonstrate that the DExH protein NPH-II from vaccinia virus can displace the protein U1A from RNA in an active adenosine triphosphate–dependent fashion. NPH-II increases the rate of U1A dissociation by more than three orders of magnitude while retaining helicase processivity. This indicates that DExH/D proteins can effectively catalyze protein displacement from RNA and thereby participate in the structural reorganization of ribonucleoprotein assemblies.

Many DExH/D proteins hydrolyze nucleoside triphosphates (NTPs) in a reaction that is stimulated by nucleic acids, and unwind RNA duplexes in an NTP-dependent fashion in vitro (*1*). DExH/D proteins are frequently part of large ribonucleoprotein (RNP) assemblies such as the spliceosome or viral replication machineries (*2, 3*). In some instances, DExH/D proteins have been shown to couple NTP hydrolysis to conformational changes in these complexes (*4–6*), and it is generally believed that this represents the predominant function of these enzymes in RNP assemblies (*2*).

Despite the importance of DExH/D proteins, little is known about the mechanisms by which these enzymes effect the numerous conformational changes that occur in RNP machines. It has been demonstrated that DExH/D proteins can function as processive and directional molecular motors for unwinding regular RNA duplexes (*7*). Although unwinding of regular duplex RNA is clearly important in RNA metabolism, cellular RNA often has a more complex structure and is likely to be bound to proteins. This fact has prompted the attractive hypothesis that DExH/D proteins might not necessarily be "pure" RNA helicases; rather, they may also function to disrupt or rearrange RNA-protein interactions (*2*). However, such activity by DExH/D proteins has never been demonstrated.

We tested the ability of DExH/D proteins to displace proteins from RNA by investigating whether the DExH protein NPH-II from vaccinia virus can displace the protein U1A from an RNA substrate (*8*). NPH-II is an RNA helicase that unwinds RNA duplexes processively in the 3′ to 5′ direction with a kinetic step size of roughly one-half helical turn (*7*). Use of a kinetically well-characterized RNA helicase permits direct comparisons of the RNA unwinding and protein displacement activities. U1A is an ideal target protein because its RNA-binding properties have been characterized (*9*). U1A binds RNA through an NH_2-terminal RNP domain (*10*), which is the most common motif for mediating specific RNA-protein interactions (*11*). The active displacement of U1A is of particular interest because it is a constituent of the spliceosomal machinery and a feedback regulator of its own gene expression.

In order to simultaneously monitor U1A displacement and RNA helicase activity, a multifunctional RNA substrate was designed. The substrate contains the U1A binding site from the 3′-untranslated region (UTR) of U1A mRNA (Fig. 1A). U1A binds this motif as a dimer, interacting primarily with two asymmetric loop

[1]Department of Biochemistry and Molecular Biophysics, Columbia University, New York, NY 10032, USA. [2]Sloan Kettering Institute, New York, NY 10021, USA. [3]Howard Hughes Medical Institute, Boston, MA 02115, USA.

*To whom correspondence should be addressed. E-mail: amp11@columbia.edu

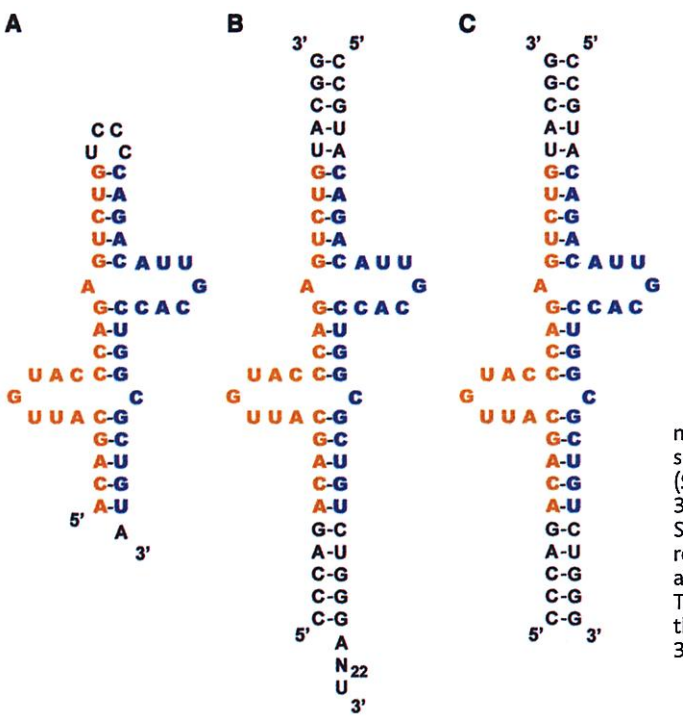

Fig. 1. Substrate design and structure of the U1A binding site. (**A**) Sequence and secondary structure of the U1A binding site in the U1A mRNA 3′ UTR (*30*). Orange and blue letters correspond to the nucleotides retained in the substrates and present in the structure (D). (**B**) Substrate. Colored letters represent nucleotides retained in the wild-type U1A binding site; black letters correspond to the nucleotides added as described in the text. The duplex regions are identical to sequences included in constructs used to study the structure of the complex (*9*). The 24 nucleotide single-strand overhang ($AN_{22}U$-3′) has the sequence 3′-UACAGUAACUACGACAAUCAUGCA. (**C**) Blunt-end control RNA. (**D**) Structure of the U1A RNA complex as determined by nuclear magnetic resonance (*12*) (Protein Data Bank accession no. 1DZ5). The two protein units are drawn as a transparent surface with ribbons representing the backbone. The two RNA strands are drawn as a ladder with the sticks corresponding to the bases and the ribbon corresponding to the backbone. The location of the 3′ end with the single-strand overhang on the RNA substrate is indicated.

structures (*12*) that are imbedded within a set of duplex motifs (*11*) (Fig. 1D). To transform the U1A binding site into a helicase substrate, the hairpin loop was removed, and the flanking helical regions were lengthened (Fig. 1B). This type of extended two-piece substrate for U1A binding has previously been shown to retain subnanomolar affinity for U1A binding (*9*). In order to promote high-affinity NPH-II binding, a single-strand 3′ overhang was appended to the duplex region (Fig. 1B) (*13*). A blunt-ended control substrate was also synthesized, which contained the U1A binding site but lacked the single-strand overhang (Fig. 1C).

U1A bound to both substrate and control RNA with high affinity (Fig. 2, A and C), demonstrating that the base-paired extensions and single-strand overhang did not alter the binding of U1A.

The U1A binding site differs substantially from regular A-form helical geometry (Fig. 1D), and there is evidence that, even without bound U1A, the RNA is extensively bent (*9*). Despite this distortion in the RNA, NPH-II

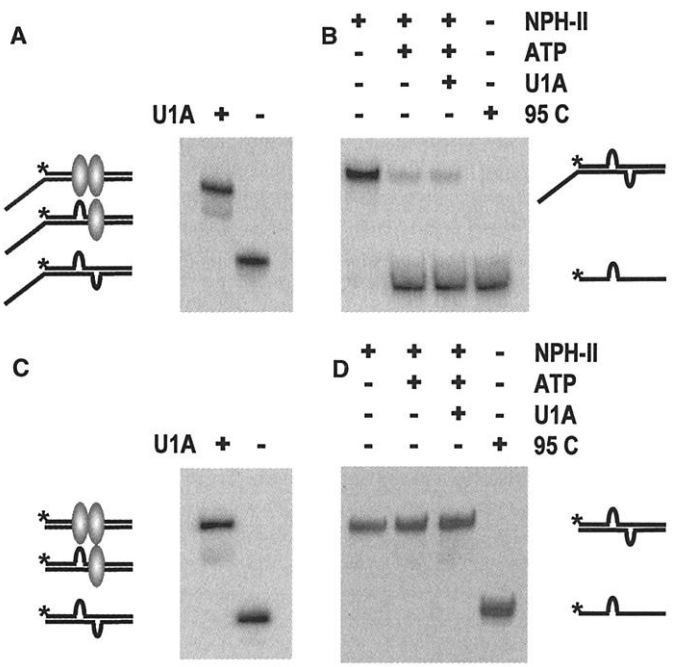

Fig. 2. U1A binding to the RNA substrate and its effects on unwinding. (**A**) U1A binding to substrate RNA (Fig. 1B). Radiolabeled substrate (1 nM) was combined with U1A (10 nM) in a buffer containing 40 mM tris-HCl (pH 8.0) and 4 mM $MgCl_2$ (in a final volume of 10 μl). After incubation at room temperature for 5 min, glycerol was added (8% v/v final) and the mixture was subjected to 8% native PAGE at 4°C, running at 10 V cm^{-1}. Bands were visualized by a PhosphorImager. Species corresponding to free substrate RNA, bound U1A monomer, and bound U1A dimer are indicated at left. The asterisk represents the radiolabel. Left lane, RNA substrate bound to U1A; right lane, free substrate. (**B**) The effect of U1A binding on duplex unwinding. Reactions were performed at room temperature for 5 min with 1 nM RNA substrate and 20 nM NPH-II in a buffer of 40 mM tris-HCl (pH 8.0); 4 mM $MgCl_2$; and, if applicable, 3.5 mM ATP (10 μl final volume). Where present, the U1A concentration was 10 nM. Substrate and U1A were preincubated for 5 min at room temperature. NPH-II was added and then incubated for 5 min more. The reaction was then started by addition of ATP. Reactions were quenched by adding 10 μl of a solution containing 25 mM EDTA, 0.4% SDS, 0.05% bromphenol blue, 0.05% xylene cyanol, and 10% glycerol. Mixtures were subjected to 15% native PAGE, which was run at room temperature at 20 V cm^{-1}. Lanes from left to right are as follows: unwinding reaction without ATP, NPH-II unwinding reaction, unwinding in the presence of 10 nM U1A, and boiled substrate. Unwound and duplex species are indicated by the cartoons at right. (**C**) U1A binding to the blunt-end control RNA. Binding reactions were performed as described and shown in (A). (**D**) Unwinding reactions with the blunt-end control RNA. Lanes correspond to those in (B).

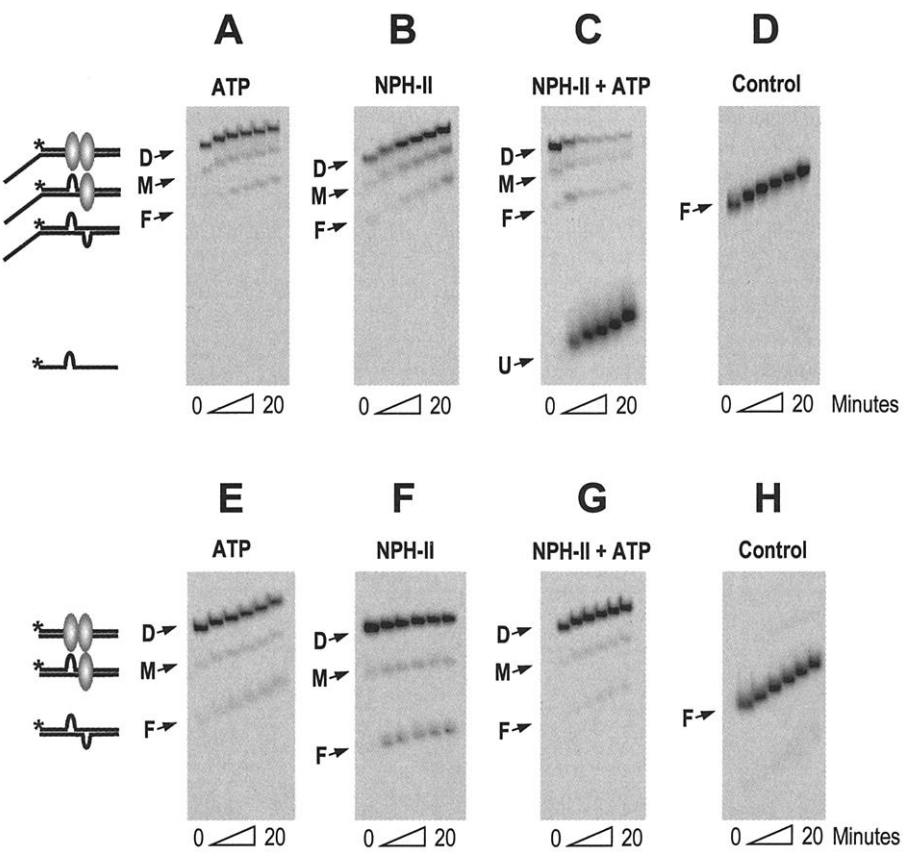

Fig. 3. Active displacement of U1A by NPH-II. Dissociation experiments were conducted with 1 nM RNA substrate and 10 nM U1A in a buffer of 40 mM tris-HCl (pH 8.0) and 4 mM $MgCl_2$ at 23°C (final volume, 40 μl). Reactions were performed as described in Fig. 2, except that they were initiated by addition of ATP (3.5 mM final concentration) and U1A trap [200 nM final concentration (*15*)], as indicated. Aliquots (6 μl) were withdrawn at 0, 1, 4, 8, 12, and 20 min and mixed with 2 μl of 100 mM EDTA and 2.5 μM NPH-II trap [which serves to capture dissociated NPH-II (*16*)] in 30% glycerol. Each aliquot was then loaded immediately on a 8% native polyacrylamide gel, which was run at 4°C at 10 V cm^{-1}. Bands were visualized by a PhosphorImager. U1A-bound and free RNA as well as unwound and duplex RNA species are indicated by the cartoons at left (D, bound U1A dimer; M, bound U1A monomer; F, U1A free duplex substrate; U, unwound substrate). (**A**) Release of U1A upon addition of ATP (initiated by adding ATP together with U1A trap). (**B**) Release of U1A upon addition of NPH-II without ATP (initiated by adding only U1A trap). (**C**) Release of U1A in the presence of ATP and NPH-II (initiated by adding ATP together with U1A trap). (**D**) Trapping control: U1A trap was added together with RNA substrate to assess trapping efficiency. Aliquots were removed and treated as described above. (**E** to **H**) Same reactions as above, but with blunt-end control duplex.

readily separated the two substrate strands in both the presence and absence of bound U1A (Fig. 2B). These findings establish that NPH-II can displace U1A. They also indicate that NPH-II can traverse loops and tolerate considerable bending in both substrate strands during duplex unwinding (*14*).

No unwinding was observed for the blunt-ended RNA substrate, regardless of whether U1A was bound (Fig. 2D). This provides two important controls: First, strand separation does not initiate at the internal loops; and second, U1A binding does not provide additional opportunities for NPH-II to initiate unwinding.

Next, it was important to distinguish whether NPH-II displaces U1A actively or in a passive manner. In the latter scenario, NPH-II would wait passively until U1A dissociates and then rearrange the binding site so that U1A can no longer bind. In an active process, NPH-II would affect the kinetics of U1A dissociation from the RNA. We reasoned that it should be possible to distinguish both processes by measuring the effect of NPH-II action on U1A dissociation rates (Fig. 3).

The off rate for U1A was measured by saturating the substrate with U1A and, after complex formation, adding a large excess of RNA that contained another high-affinity U1A binding site (*15*). This prevented U1A from rebinding the substrate once it detached and enabled us to monitor the rate of U1A release by gel-shift electrophoresis (Fig. 3).

Without NPH-II, roughly 15% of U1A dissociates from the substrate within 20 min, which corresponds to an off rate of $k_{off} \sim 10^{-2}$ min^{-1} (Fig. 3A). In the presence of NPH-II, but without adenosine triphosphate (ATP), no unwinding is observed (compare Fig. 1B) and the off rate was not significantly changed (Fig. 3B), which indicates that U1A is not displaced by mere binding of NPH-II to the substrate. However, adding both NPH-II and ATP resulted in a dramatically increased off rate for U1A (Fig. 3C). After only 4 min, U1A was almost completely released from the substrate. This suggests a rate increase of several orders of magnitude and clearly demonstrates that NPH-II dissociates U1A from the substrate in an active energy-dependent fashion.

The rate of U1A dissociation from the blunt-end RNA is similar to the rate of U1A dissociation from the helicase substrate in the absence of NPH-II (Fig. 3E) or in the presence of NPH-II without ATP (Fig. 3F). However, unlike the helicase substrate, NPH-II combined with ATP does not increase the rate of U1A dissociation (Fig. 3G). Thus, displacement of U1A by NPH-II is not caused by the structural peculiarities of the U1A binding site but rather depends on binding of NPH-II to the single-strand overhang of the substrate.

Having established that NPH-II actively displaces U1A in an ATP-dependent fashion, it was of interest to determine how U1A binding impedes the helicase activity of NPH-II and to obtain a kinetic framework for the process of protein displacement by a DExH/D protein. To this end, U1A displacement was monitored under single-cycle conditions with respect to NPH-II; that is, any NPH-II that dissociates from the RNA cannot rebind. This was achieved by adding a large excess of trap RNA together with the ATP that is used to initiate unwinding of the NPH-II/substrate/U1A complex (*16*). In this manner, it was possible to monitor the relative fractions of U1A-bound RNA substrate, free duplex substrate, and unwound RNA strands (Fig. 4A). Although the decay of substrate bound to U1A was first order (*17*), the fraction of free duplex substrate passed through a maximum and the fraction of unwound substrate evolved with a small lag phase (Fig. 4, A and C). This indicates a sequential reaction and suggests the presence of a second slow step after U1A has been displaced.

The most important observation, however, was that a sizable fraction of the substrate was unwound by NPH-II under single-cycle conditions; i.e., NPH-II was able to displace U1A and continue unwinding the substrate without necessarily falling off during the course of reaction. Thus, processivity was not eliminated by the binding of U1A. Nevertheless, U1A caused substantial defects in the

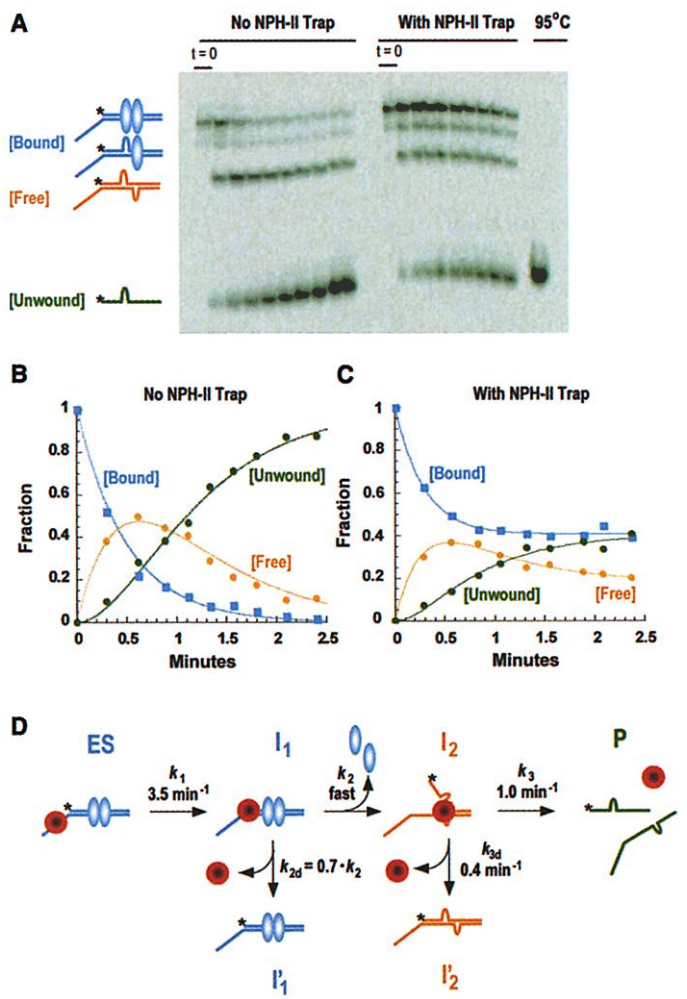

Fig. 4. Mechanism of U1A displacement by NPH-II. (**A**) Time course of U1A displacement and substrate unwinding with and without NPH-II trap. Reactions without NPH-II trap were conducted as described in Fig. 3. The reaction with NPH-II trap was initiated by adding a combination of ATP (3.5 mM final concentration), U1A trap (200 nM final concentration), and NPH-II trap (500 nM final concentration). Aliquots were withdrawn at the times indicated in the plots [(B) and (C)]. U1A-bound, free substrate, and unwound substrate species are indicated by the cartoons at left (bound, U1A dimer and monomer; free, nonbound and nonunwound substrate; unwound, unwound substrate). (**B**) Plot of reaction without NPH-II trap for bound, free, and unwound substrate [under normalized (*26*) multiple cycle conditions]. The monomer and dimer forms of bound U1A decayed at roughly the same rate and were therefore combined as the bound fraction. Solid lines are the simulated fits of the data based on the reaction mechanism described below (*19*), using the emipirically determined rate constants (D). (**C**) Plot of reaction with NPH-II trap (single-cycle conditions). Solid lines are the best fit to the integrated rate laws derived from the mechanism below (*17*). (**D**) Kinetic mechanism of U1A displacement and unwinding by NPH-II. The red circle represents NPH-II, and the blue elipsoids represent U1A. Rate constants were calculated according to integrated rate laws describing single-cycle reaction kinetics (*17*), using three different time courses (C). Abbreviations are as follows: *ES*, NPH-II–substrate–U1A complex before reaction initiation; I_1, NPH-II–U1A–substrate complex after the first rate-limiting step; I'_1, substrate-U1A complex (after NPH-II dissociation); I_2, NPH-II–substrate complex (after U1A displacement); I'_2, substrate (after U1A displacement and NPH-II dissociation); P, unwound product. At the end of the reaction, NPH-II dissociates rapidly and irreversibly from the substrate. The fraction of substrate bound to U1A consists of the species *ES*, I_1, and I'_1. The fraction of free substrate comprises I_2 and I'_2.

processivity of NPH-II, as indicated by a plateau in the decay of bound U1A, the fact that the amplitude of free substrate did not return to zero, and the fact that unwinding did not go to completion but only to roughly 40% (Fig. 4, A and C). Taking all these observations together, it was possible to derive explicit equations describing the time courses and to model a basic kinetic mechanism for the reaction (Fig. 4D) (*17*).

In this mechanism, NPH initiates the displacement/unwinding reaction with a rate constant of $k_1 = 3.5\ \text{min}^{-1}$. This rate constant is identical to that of the rate-limiting step for unwinding a regular duplex during the NPH-II helicase reaction, which involves a slow step at the junction between the single-strand overhang and the duplex region (*7*). After this initiation step, NPH-II proceeds to displace U1A. This step is fast compared to the initiation step. The actual rate for U1A displacement is therefore kinetically invisible. However, a lower limit for U1A displacement of $k_2 > 50\ \text{min}^{-1}$ can be estimated (*18*), which is more then three orders of magnitude faster than the rate of U1A dissociation in the absence of NPH-II and ATP ($\sim 10^{-2}\ \text{min}^{-1}$). Even before U1A is displaced, NPH-II dissociates with a rate of $0.7 \cdot k_2$, which explains why only ~60% of U1A molecules are released. After U1A is displaced, another slow step occurs ($k_3 = 1\ \text{min}^{-1}$), in which a fraction of NPH-II dissociates from the substrate ($k_{3d} = 0.4\ \text{min}^{-1}$). This second slow step (k_3) is strictly dependent on the presence of U1A and was not observed during unwinding of the substrate without U1A (*14*). The kinetic steps above are likely to describe composite processes; i.e., the rate constants do not necessarily reflect microscopic reaction steps. Analysis of unwinding/displacement under multiple cycle conditions [in which dissociated NPH-II can rebind the substrate (*19*) (Fig. 4A, left panel)] indicated that no additional rate-altering steps other than rebinding events affect the reaction (Fig. 4B).

Four major mechanistic insights follow from the kinetic analysis: First, physical displacement of U1A is not the slowest step in the reaction, despite the high affinity of U1A to the substrate. Second, NPH-II increases the dissociation rate of U1A by more then three orders of magnitude. Third, NPH-II retains a significant level of processivity while displacing U1A. Fourth, after U1A is displaced, NPH-II needs to be reoriented or repositioned in order to complete substrate unwinding, as suggested by the second slow step (k_3). There are at least two models by which NPH-II accelerates the dissociation of U1A protein: NPH-II may alter the conformation of RNA around the U1A binding site, or it may directly "plow" U1A off the RNA. Although the methods used here cannot distinguish these scenarios, the presence of intermediate species I_2 (Fig. 4D) indicates that U1A displacement does not require the complete unwinding of the RNA duplex, thereby suggesting that a form of "snowplow" model is possible.

By showing that NPH-II actively displaces U1A, this study establishes that DExH/D proteins are capable of efficiently dislodging other proteins from RNA molecules. This RNP displacement, or "RNPase" function, is a form of enzymatic activity that is driven by ATP hydrolysis and which, like RNA helicase activity, is likely to have many different manifestations in cellular RNA metabolism. The observation that helicase processivity is not eliminated during U1A displacement suggests that DExH/D proteins may be able to switch back and forth between helicase and protein displacement functions, indicating that both activities can reside in the same protein and can function in the same macromolecular context (*20*). By obviating the need for numerous additional cofactors, this function may considerably simplify the requirements for RNP disassembly or rearrangement during processes such as pre-mRNA splicing or ribosome assembly.

References and Notes

1. J. de la Cruz, D. Kressler, P. Linder, *Trends Biochem. Sci.* **24**, 192 (1999).
2. J. P. Staley, C. Guthrie, *Cell* **90**, 1041 (1998).
3. G. Kadare, A. L. Haenni, *J. Virol.* **71**, 2583 (1997).
4. B. Schwer, C. Guthrie, *EMBO J.* **11**, 5033 (1992).
5. P. L. Raghunathan, C. Guthrie, *Curr. Biol.* **8**, 847 (1998).
6. J. D. O. Wagner, E. Jankowsky, M. Company, A. M. Pyle, J. N. Abelson, *EMBO J.* **17**, 2926 (1998).
7. E. Jankowsky, C. H. Gross, S. Shuman, A. M. Pyle, *Nature* **403**, 447 (2000).
8. U1A containing residues 1 through 117 was expressed and purified as described (*21*). NPH-II was expressed in cultured insect cells infected with recombinant baculovirus and purified as described (*22*). The purity of both proteins (>95%) was assessed by polyacrylamide gel electrophoresis (SDS-PAGE) and staining of the polypeptides with Coomassie brilliant blue.
9. R. J. Grainger, D. G. Norman, D. M. Lilley, *J. Mol. Biol.* **288**, 585 (1999).
10. D. Scherly, W. Boelens, N. A. Dathan, W. J. van Venrooij, I. W. Mattaj, *Nature* **345**, 502 (1990).
11. G. Varani, K. Nagai, *Annu. Rev. Biophys. Biomol. Struct.* **27**, 407 (1998).
12. L. Varani *et al.*, *Nature Struct. Biol.* **7**, 329 (2000).
13. To unwind RNA, NPH-II requires a single-strand overhang 3′ to the duplex region (*23*). Optimal helicase activity requires a 3′ overhang of at least 20 nucleotides (*24*). The affinity of NPH-II for blunt-end duplex RNA is low; no significant binding is observed at nanomolar concentrations of NPH-II (*24*).
14. Unwinding of substrate in the absence of U1A can be described by a single exponential with a rate constant of $k_{\text{unwinding}} = 3.5 \pm 0.4\ \text{min}^{-1}$, which is in agreement with rate constants measured for unwinding of regular duplexes under these conditions (*7*). In the presence of NPH-II trap, ~70% of substrate was unwound; i.e., the overall processivity for unwinding this substrate is slightly lower then the overall processivity for unwinding a regular duplex with the same number of base pairs (bp) (*7*). U1A did not affect unwinding reactions with regular duplexes at the concentrations used (*24*).
15. The RNA used for trapping dissociated U1A was based on the hairpin that forms the U1A binding site in the U1 small nuclear RNA (*10*). An RNA oligonucleotide of the sequence 5′-GGAGAACCAUUGCACUCCGGUUCUUC was prepared by chemical synthesis and purified as described (*25*).
16. NPH-II trap consisted of a 12-bp duplex with a 24-nucleotide single-strand overhang that was formed out of two strands with the sequence 3′-ACGAGGGAGACGAGGAGACGGAGCGACGGCAGCGGU and 5′-CUGCCGUCGCCA. RNAs were synthesized and purified, and the duplex was formed as described (*7*, *25*).
17. Explicit equations describing the kinetic mechanism (Fig. 4D) were derived by considering the species I_1 as a fast intermediate such that $dI_1/dt = 0$. The relative fractions (frac) of bound, free, and unwound substrate were described by

$$\text{frac[bound]} = \frac{k_{2d}}{k_2 + k_{2d}} \cdot (1 - e^{-k_1 t}) + e^{-k_1 t}$$

$$\text{frac[free]} = \frac{k_2}{k_2 + k_{2d}} \cdot \left[\frac{k_1}{k_3 + k_{3d} - k_1} \cdot \frac{k_3}{k_3 + k_{3d}} \cdot (e^{-k_1 t} - e^{-(k_3 + k_{3d})t}) + \frac{k_{3d}}{k_3 + k_{3d}} (1 - e^{-k_1 t}) \right]$$

$$\text{frac[unwound]} = \frac{k_2}{k_2 + k_{2d}} \cdot \frac{k_3}{k_3 + k_{3d}} \cdot \left[1 - e^{-k_1 t} - \frac{k_1}{k_3 + k_{3d} - k_1} \cdot (e^{-k_1 t} - e^{-(k_3 + k_{3d})t}) \right]$$

where t is time. These equations were used to fit the normalized (*26*) time courses of reactions conducted in the presence of NPH-II trap RNA. Fitting was performed with Kaleidagraph (Synergy software). Values for $k_2/(k_2 + k_{2d})$ and for k_1 were obtained by fitting the time course of fraction[bound]. Values for k_3 and k_{3d} were computed by fitting fraction[free] and fraction[unwound] with fixed k_2/k_{2d} and k_1. The rate constants provided are average values calculated from three different time courses, resulting in $k_1 = 3.52 \pm 0.15\ \text{min}^{-1}$, $k_2/(k_2 + k_{2d}) = 0.59 \pm 0.02$, $k_3 = 1.04 \pm 0.04\ \text{min}^{-1}$, and $k_{3d} = 0.40 \pm 0.12\ \text{min}^{-1}$.
18. The lower limit for k_2 was estimated by simulating the time course with the empirically determined rate constants but decreasing the values for k_2. Noticable deviation from the observed time course was detected for values of $k_2 < 50\ \text{min}^{-1}$; i.e., the actual constant k_2 is necessarily larger than this value.
19. For simulating the reaction without NPH-II trap, rebinding of helicase to substrate was considered by adding three steps to the reaction scheme in Fig. 4D. (i) Fast binding of helicase to substrate-U1A complex: $E + I'_1 \rightarrow ES$, where $k_6 = 10^9\ \text{mol}^{-1} \cdot \text{min}^{-1}$ and the initial NPH-II concentration $E_0 = 20$ nM. (ii) Fast rebinding of helicase to substrate, without U1A bound: $E + I'_2 \rightarrow EI'_2$, where $k_7 = 10^9\ \text{mol}^{-1} \cdot \text{min}^{-1}$ and the initial NPH-II concentration $E_0 = 20$ nM. (iii) Unwinding of rebound substrate without U1A bound: $EI'_2 \rightarrow P$, where $k_8 = 3.5\ \text{min}^{-1}$ (*14*). Step (iii) represents multiple reactions. Simulations were performed with normalized (*26*) time courses using the KINSIM software package (*27*).
20. This contrasts with the SNF2 family protein Mot1p, which displaces the TATA box–binding protein from DNA in an ATP-dependent fashion (*28*) but lacks helicase activity.
21. J. M. Avis *et al.*, *J. Mol. Biol.* **257**, 398 (1996).
22. C. H. Gross, S. Shuman, *J. Virol.* **69**, 4727 (1995).
23. S. Shuman, *J. Biol. Chem.* **268**, 11798 (1993).
24. E. Jankowsky *et al.*, unpublished results.
25. RNA oligonucleotides were prepared by chemical synthesis on an ABI 392 RNA/DNA synsthesizer using phosphoramidite chemistry (reagents were purchased from Glen Research, Sterling, VA). Crude oligonucleotides were deprotected according to standard protocols (*29*) and purified by denaturing PAGE. Duplexes were formed and purified as described previously (*7*).
26. Amplitudes were corrected for the final reaction endpoint (normalized). Endpoints ($t \rightarrow \infty$) were determined after 10 min of reaction without NPH-II trap. The endpoint values were determined to be as follows: $\text{frac[bound]}_{obs}(t \rightarrow \infty) = 0.04$, $\text{frac[free]}_{obs}(t \rightarrow \infty) = 0.02$, and $\text{frac[unwound]}_{obs}(t \rightarrow \infty) = 0.94$. Amplitudes at a given t were corrected as follows: $\text{frac[bound]}(t) = (\text{frac[bound]}_{obs}(t) - 0.04)/(1 - 0.04)$, $\text{frac[unwound]}(t) = \text{frac[unwound]}_{obs}(t)/0.94$, $\text{frac[free]}(t) = 1 - \text{frac[bound]}(t) - \text{frac[unwound]}(t)$.
27. B. A. Barshop, C. Frieden, *Anal. Biochem.* **130**, 134 (1983).

28. D. T. Aubele, D. Wang, K. W. Post, S. Hahn, *Mol. Cell Biol.* **17**, 4842 (1997).
29. F. Wincott *et al.*, *Nucleic Acids Res.* **23**, 2677 (1995).
30. C. W. van Gelder *et al.*, *EMBO J.* **12**, 5191 (1993).

31. We thank K. Nagai for supplying purified U1A protein and for helpful discussion and S. Lomvardas for advice and assistance in visualizing RNA-protein complexes. Supported by grants from the NSF (NSF Young Investigator Award to A.M.P.) and the Matheson Foundation (A.M.P.). A.M.P. is an assistant investigator of the Howard Hughes Medical Institute.

13 October 2000; accepted 17 November 2000

Effectiveness of Parks in Protecting Tropical Biodiversity

Aaron G. Bruner,[1]* Raymond E. Gullison,[2] Richard E. Rice,[1] Gustavo A. B. da Fonseca[1]

We assessed the impacts of anthropogenic threats on 93 protected areas in 22 tropical countries to test the hypothesis that parks are an effective means to protect tropical biodiversity. We found that the majority of parks are successful at stopping land clearing, and to a lesser degree effective at mitigating logging, hunting, fire, and grazing. Park effectiveness correlates with basic management activities such as enforcement, boundary demarcation, and direct compensation to local communities, suggesting that even modest increases in funding would directly increase the ability of parks to protect tropical biodiversity.

Much of tropical biodiversity is unlikely to survive without effective protection (*1–3*). Conservationists have tried strategies ranging from establishing and maintaining parks and other strictly protected areas (henceforth "parks"), to promoting sustainable forest management and other integrated conservation and development projects. How well do parks measure up among these alternatives (*4*, *5*)? Critics claim that in the context of growing human pressures and development needs, parks cannot protect the biological resources within their borders (*6*), and there is a widespread sense that parks are simply not working. The accuracy of these claims is of critical importance to policy and funding decisions. If parks are failing despite best efforts, then better options should be sought. If, on the other hand, parks are performing relatively well in a context of serious threats and limited resources, or are simply performing better than the alternatives, their level of support should be increased.

Past studies of park effectiveness have focused on improving park management (*7*), improving protected area system design (*8*), and increasing local and national political support (*9*, *10*), but none has provided a quantitative assessment of effectiveness using a large sample of parks around the world (*11*, *12*).

We used a questionnaire to collect data on land-use pressure (land clearing, logging, hunting, grazing, and fire), local conditions (e.g., presence of human communities in parks and degree of access), and management activities (e.g., number of guards and level of community involvement in management) (*13*). To confine our sample to parks at risk of failure, we selected regions subject to significant human land-use pressure (*14*, *15*). From these regions, we selected only parks that have been established for at least 5 years to allow sufficient time for management activities to be reflected in park performance. We also restricted the sample to protected areas of >5000 ha in which only nonconsumptive uses were permitted (*16*, *17*). Directors of conservation organizations and protected area agencies helped identify a representative group for this study from the 535 parks that met these criteria (*18*, *19*) [additional information is available on *Science* Online (*20*)]. The sample comprised 93 parks (*21*) in 22 countries (*22*), covering 17% (18 million ha) of the parks that met our criteria (*23*).

The parks in the sample varied greatly in size, primary ecosystem type, budget, management strategy, and type and degree of threats. Seventy percent had people living inside their boundaries, and 54% had residents who contested the ownership of some percentage of the park area. Two-thirds of the parks were accessible by at least one major road or river (*24*). Median annual funding was 1.18 USD ha^{-1}, significantly less than the amount often recommended for effective management (*25*). Finally, respondents judged that many park staff were lacking in critical training and equipment.

We assessed the effectiveness of these parks from three perspectives: land clearing within the boundaries of parks since establishment, current condition of parks compared with the condition of their surroundings, and factors correlated with effective park protection.

We assessed the effectiveness of parks at preventing land clearing by comparing the current extent of clearing with clearing at the time of park establishment (Fig. 1). We found that 43% of the parks have had no net clearing since establishment. In an additional 40% of parks, land formerly under cultivation was incorporated into park boundaries, and had been able to recover, leading to an actual increase in vegetative cover. Eighty-three percent of parks were therefore fully holding their borders against agricultural encroachment. Only 17% of the parks experienced net clearing since establishment. This is a substantial achievement, given that the median age of the parks in our sample is 23 years.

To test effectiveness over a wider range of threats, we compared anthropogenic impacts in the 10-km belt surrounding parks with the level of impacts within park boundaries for five different threats (Fig. 2). This comparison shows that the parks in our sample are under great pressure from clearing, hunting, and logging, and to a lesser extent, fire and grazing. A comparison of the conditions inside the parks with the surrounding area shows that for all five threats, parks were in significantly better condition than their surrounding areas (Mann-Whitney U-test, medians significantly different at

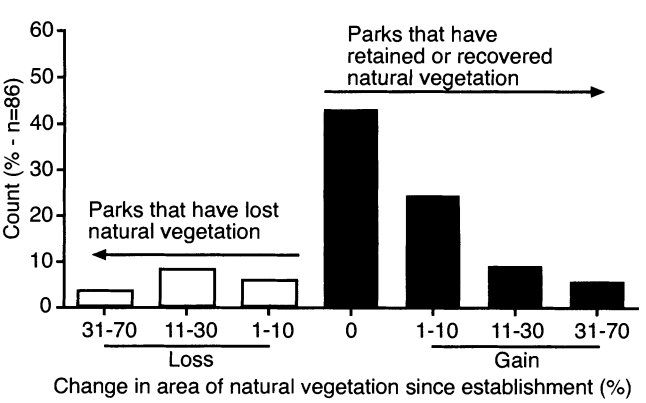

Fig. 1. Change in the area of natural vegetation since establishment for 86 tropical parks. The majority of parks have either experienced no net clearing or have actually increased natural vegetative cover. Median park age is 23 years.

[1]Center for Applied Biodiversity Science at Conservation International, 2501 M Street, NW, Suite 200, Washington, DC 20037, USA. [2]Centre for Biodiversity Research, University of British Columbia, 6270 University Boulevard, Vancouver, British Columbia V6T 1Z4, Canada.

*To whom correspondence should be addressed. E-mail: a.bruner@conservation.org